C Journal of Carbon Research

MDPI

Article

Carbon Nanofibers Grown on Large Woven Cloths: Morphology and Properties of Growth

Vitaly Koissin [1], Ton Bor [1], Željko Kotanjac [2], Leon Lefferts [2], Laurent Warnet [1] and Remko Akkerman [1,*]

[1] Production Technology Group, Department of Mechanical Engineering, University of Twente, 7500 AE Enschede, The Netherlands; vitaly@kth.se (V.K.); t.c.bor@utwente.nl (T.B.); l.warnet@utwente.nl (L.W.)

[2] Catalytic Processes and Materials Group, Department of Chemical Engineering, University of Twente, 7500 AE Enschede, The Netherlands; z.kotanjac@misc.utwente.nl (Ž.K.); l.lefferts@utwente.nl (L.L.)

* Correspondence: r.akkerman@utwente.nl; Tel.: +31-053-489-2566

Academic Editor: Craig E. Banks

Received: 26 April 2016; Accepted: 13 June 2016; Published: 4 July 2016

Abstract: The morphology and chemical composition of carbon nanofibers in situ grown on a large carbon-fiber woven fabric are studied using SEM measurements, X-ray Diffraction, X-ray Flourescence, and X-ray Photoelectron Spectroscopy. Results show that nanofibers can have a density and a morphology potentially advantageous for application in polymer-matrix composites. The fiber surface functional groups significantly change after the growth and this also potentially provides a better interfacial adhesion. These advantages can be controlled, e.g., by the catalyst loading and the type of solvent used for its deposition.

Keywords: fabrics; CVD; carbon nanofibers; morphology; chemical properties

1. Introduction

Recent reviews, [1], illustrate significant efforts to employ in situ grown carbon nanotubes (CNTs) and carbon nanofibers (CNFs) to improve the fiber-matrix interface in continuous carbon fiber reinforced plastics (CFRPs). Successful application of this approach can extend the applicability of CFRPs by improving the fiber-matrix bonding and micro-crack bridging and, consequently, by increasing the allowable load and damage resistance of the composite materials.

There are a few methods of introducing CNTs or CNFs into a CFRP. In the present study CNFs are grown directly on a carbon-fiber fabric by the catalytic decomposition of a hydrocarbon gas onto Ni particles [2], using the Chemical Vapor Deposition (CVD). This method potentially promotes a homogeneous distribution of the CNFs in the fabric as well as their good bonding to the fibers. The method is chosen because the in situ growth of CNFs has received little (in comparison with CNTs) attention in studies published so far, as reviewed in [2], though CNFs can probably bring a larger benefit. Also, growth of CNTs usually requires higher temperatures (and therefore more expensive equipment, though moderate temperature CNT synthesis has also been reported, [3]) and well-defined process conditions (which are hardly realizable in a mass production of CNT-grafted textiles).

This paper reports about the resulting morphology (CNF sizes, shapes, etc.) and the final chemical state of the fabric, after the in situ growth of CNFs. Similar has already been investigated for chemically treated fibers, e.g., [4,5], for aramide fibers "sized" with CNTs [6], for carbon fibers with in situ grown CNTs [7–9] or CNFs [10–12]. It was shown that different process conditions (temperature, time, catalyst loading...) have strong impacts on the morphology and chemical properties. The present study aims to investigate this for the CNF growth on a large carbon-fiber fabric (26 × 31 cm^2), because in almost all known studies the CVD is performed in quartz tubes for small specimens, and the use of large

reactors (suitable to grow CNFs on the component level) can apply some specifics. Special attention is paid to chemical changes of the fabric surface, since this is still not widely investigated for the in situ grown CNFs.

2. Materials and Methods

2.1. Substrate

A typical woven carbon reinforcement (supplied by Ten Cate Advanced Composites B.V., Nijverdal, The Netherlands) was used: a 5-harness satin weave with a 285 g/m^2 areal weight, made of 3K non-twisted tows of Torayca T300J 7 µm diameter fibers. Three variants of this fabric were used:

(1) "Sized" fabric (TenCate CD 0286 050 000 0000) having the original Torayca standard sizing by about 1% of the fabric weight [13]. This fabric is suitable for impregnation with an epoxy matrix. The sizing has many functions; for the carbon fibers the main one is to prevent their damage during winding, prepregging, or weaving operations [14]. In the present case the exact chemical composition of the sizing is unknown but it is based on an uncured epoxy. Its typical appearance is shown in Figure 1a, where it bonds together many fibers.

(2) "Base" fabric (TenCate CD 0286 050 000 8212) which is the "sized" fabric partially de-sized for a better compatibility with a PPS matrix. Essentially, there are two methods: (a) heating at 330–430 °C for 2–4 h or (b) heating at 380–520 °C for 15 ± 5 min and then at 190–250 °C for 3–5 h. It is important that "... the carbon fibers remain unaffected and the epoxy material is aged or neutralized and loses its tacky character" [15]. This means that the sizing is just "neutralized" but not removed completely. This fabric is used as the substrate material for CNF growth for most of the tests presented in this paper.

(3) "Desized" fabric prepared by heating the "base" one up to 400 °C or 600 °C in N_2 atmosphere for about 30 min. It is used solely to reveal the effect of the high temperature, without any CNF growth. Weighing of the samples before and after this treatment shows a 0.5% weight loss. As seen in Figure 1b, the sizing is indeed not removed completely but rather carbonized forming a sort of sintered incrustation.

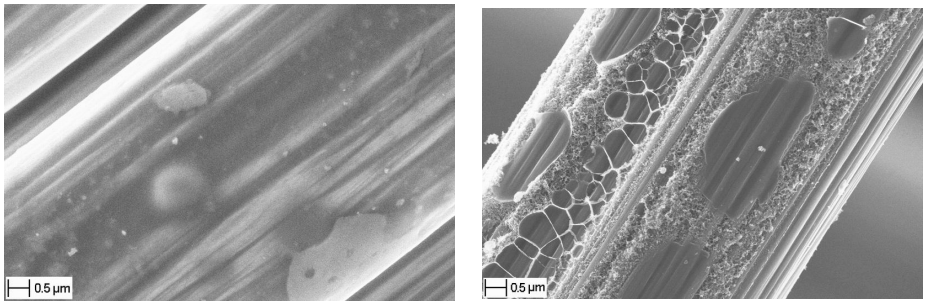

(**a**) (**b**)

Figure 1. Fibers with the original Torayca sizing (**a**) and fibers in the "desized" fabric (**b**).

2.2. Chemical Vapor Deposition

Details of the CNF growth process are described in [2]. It was performed using the Chemical Vapor Deposition (CVD) technique at the Catalytic Processes and Materials group of the University of Twente. First, the base fabric (26 × 31 cm^2 sheet) was impregnated with nickel nitrate dissolved in water or acetone. This was achieved by spraying the $Ni(NO_3)_2$ solution over the fabric; this method was shown to result in the most homogeneous distribution of CNFs, at that the acetone solution (due to its fast evaporation) resulted in the shortest production time as well as (due to specific surface tension and polarity) produced more homogeneous CNF "forest" [2].

After the impregnation the fabric was dried and placed into a gas chamber, where $Ni(NO_3)_2$ was reduced with hydrogen at 600 °C to obtain Ni particles needed for CNF synthesis (about 30 min). Subsequently, the CNFs were grown at the same temperature in a hydrocarbon gas mixture for a certain reaction time (5–10 min). Normally a 2%–3% growth (by weight) required about 5 min. Keeping the same temperature regime and gas composition, the CNF weight fraction (wt %) was controlled by varying the reaction time; only several specimens mentioned in Section 3.1 were prepared by varying the Ni concentration instead of time. In general, the weight fraction increased by an increase of the length of existing CNFs rather than by the formation of new CNFs.

The wt % is calculated as $100 \times (M_N - M_0)/M_N$, where M_0 and M_N are the initial and after-growth weights of the specimen, respectively. It should be noted that the used balance provides a 0.1 g precision, while the average mass of a 26×31 cm^2 specimen is about 21 g. Then, e.g., 5 wt % of CNFs corresponds to about 1 g which means that the wt % of CNFs is calculated with a 10% precision (5% $\pm$ 0.5% wt %). It should also be noted that the changes in weight not only account for the grown CNFs, but also include some weight gain due to the presence of Ni catalyst (0.7 wt %) and some weight loss due to "desizing" (0.5 wt %).

2.3. Test Eqiupment

XRD measurements were performed on a Panalytical Xpert 1 diffractometer (PANalytical B.V., Almelo, The Netherlands) employing Co radiation and a Fe incident beam filter, for the samples where acetone or water was used as solvent. The sample size was typically 2×2 cm^2 with a sample thickness of approximately 0.25 mm.

XRF tests were performed using a PW1480 spectrometer (Philips N.V., The Netherlands) for three specimens, about 8×8 mm^2 sized: the base fabric and two different CNF-grafted fabrics (1.4 or 7.1 wt %) prepared using the acetone solution.

XPS tests were performed with a Quantera SXM device (Physical Electronics, Chanhassen, MN, USA), for the sized fabric and for its three modifications: (1) "desized" at 400 °C; (2) "desized" at 600 °C; or (3) a 1.4 wt % grafted (the same as used above for XRF). The specimen area was about 600×300 μm^2.

3. Results

3.1. Meso- and Micro-Level Uniformity of the Growth

The thickness of the grown CNF "forest" and its morphology (density, uniformity, etc.) are important for the production of a composite part. For example, a too thick and rigid "forest" can resist bringing closer the neighboring fibers. In this case, a higher production pressure is needed to achieve the target fiber volume fraction.

In the present study, several fabrics are investigated for the influence of Ni loading and the time of growth on the resulting "forest". Figure 2 shows typical SEM images of CNF-grafted fibers after employing the acetone solution having the Ni concentration as indicated. It is seen that the CNF distribution is mostly uniform, both for relatively low (5 wt %) and high (more than 10 wt %) growths.

However, it is seen directly in Figure 2b,c that the high CNF growth produces "forest" thickness of the same order of magnitude as the fiber diameter. Therefore, as mentioned above, a high fiber volume fraction is hardly achievable in such specimens.

There is another reason for the specimens containing high CNF wt % not to be practical for real composite production and application: a prominent "expansion" of the yarns occurs when a large amount of CNFs is grown inside them. On the meso-level this results in a visible distortion of the original unit cell structure (barrel-like yarns squeezed by each other), cf. Figure 3a,b. In turn, the growth-induced internal stresses also result in a distortion of the overall shape of the specimen; it changes from a flat and flexible state to a corrugated and rigid state.

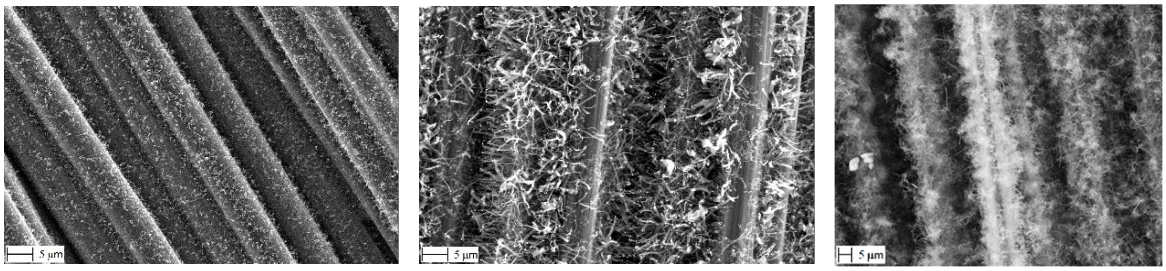

(**a**) (**b**) (**c**)

Figure 2. Typical SEM images of grafted fibers: 5 wt % (**a**) and about 10–20 wt % (**b**,**c**).

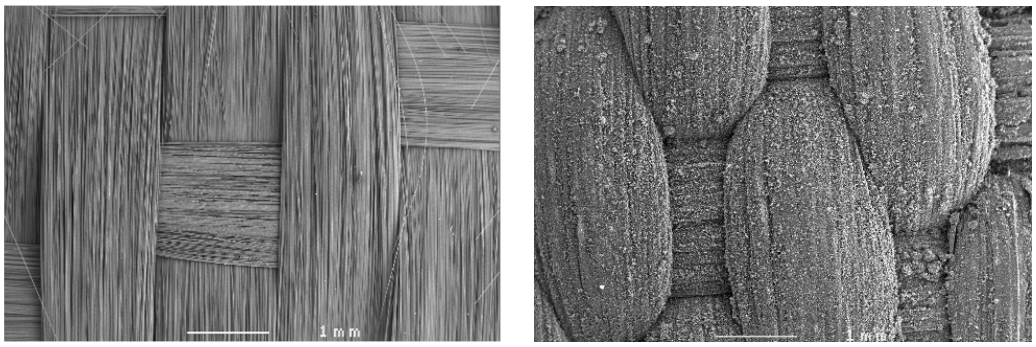

(**a**) (**b**)

Figure 3. Base (**a**) and highly grafted ((**b**), after a high 2.9 wt % Ni loading with acetone solution) fabrics.

Another test case was to grow the same CNF wt % while varying the Ni concentration in the acetone solution. Representative SEM images are shown in Figure 4 and reveal that low Ni loadings produce thinner CNFs. Higher Ni loadings result in thicker CNFs, which are sometimes even a few hundred nanometers thick, probably caused by larger Ni particles. It is also seen that the latter case results in another nucleation and growth mechanism, where a relatively uniform "forest" is changed into agglomerates with a size similar to the fiber diameter.

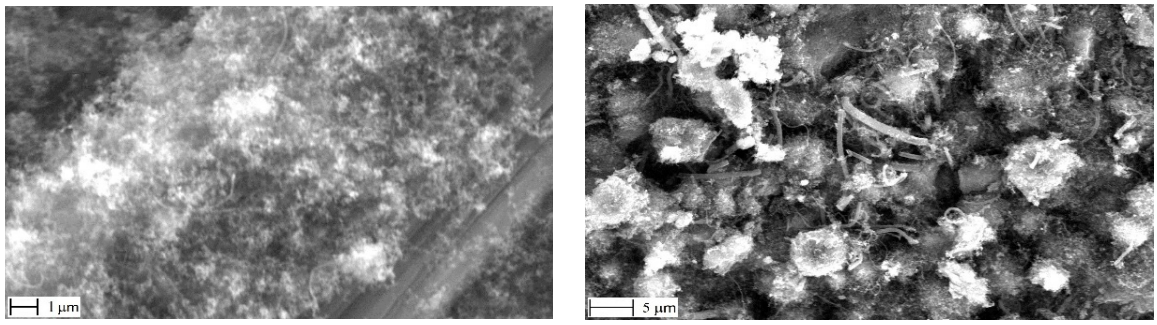

(**a**) (**b**)

Figure 4. CNF "forests" after a relatively low (0.18 wt %, (**a**)) or high (2.9 wt %, (**b**)) Ni loadings.

3.2. Nano-Scale Morphology of the Growth

Typical SEM images reveal that the CNF growth results in a spaghetti-like structure, Figure 5. The CNFs are strongly entangled, randomly shaped and sized. There are large CNFs (diameter about 100 nm or even thicker) as well as thin (5–20 nm diameter) objects. The latter, as observed in TEM images [16], can also be recognized as CNFs.

SEM images reveal also that the Ni particles are positioned mostly at the ends of CNFs. However, Ni particles can appear in other positions along CNFs, as seen in Figure 5b, where a single particle gives birth to two CNFs of similar diameters. A prominent particle fragmentation is seen in these points, where new bunches of thinner CNFs can appear, Figure 5c.

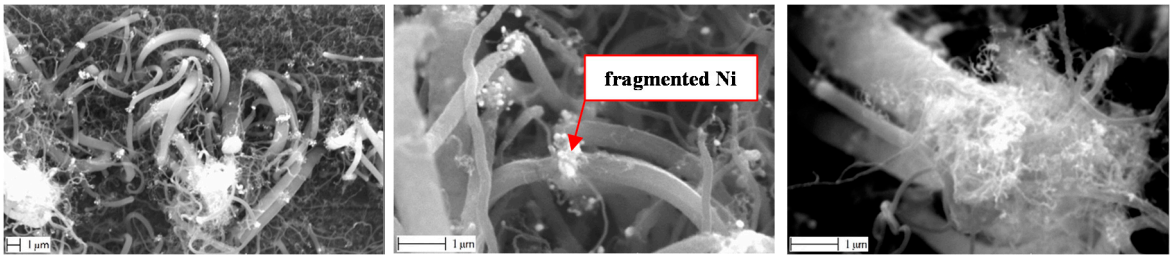

(**a**) (**b**) (**c**)

Figure 5. Typical SEM images of CNFs, after acetone solution: overall view (**a**) and larger magnifications (**b**,**c**).

As will be seen below, the randomization of sizes can be attributed to the fact that the Ni particle size is not well-controlled (even before the fragmentation) and shows a broad distribution after the used catalyst deposition methods. There are methods to obtain Ni nanoparticles of similar sizes (e.g., using microemulsion, [17,18]), but it is difficult (and for large specimens also expensive) to implement them on an industrial scale.

It seems that CNFs are strongly attached to the microfibers. As a qualitative assessment, an ultrasonic bath treatment was performed and showed that no more than 3%–5% of CNFs were removed, see also [19]. Examples of CNF attachments are shown in Figure 6. The largest CNF in the left figure gives also a good illustration of the fish-bone structure. The fishbone type of CNFs is probably better suited for interaction with a polymer, since their surfaces consist of graphene edges, which are chemically more reactive in comparison with a "smooth" surface of the tube-type CNTs.

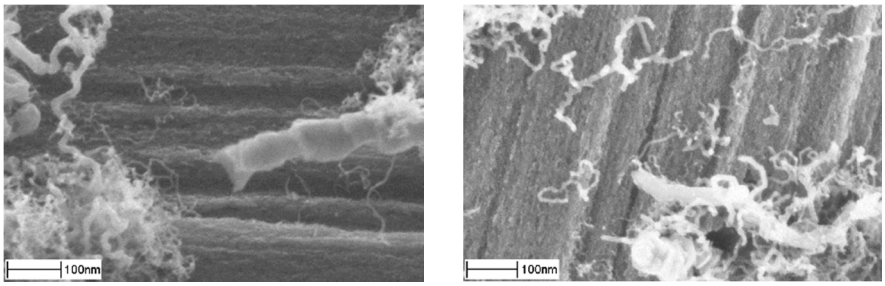

Figure 6. Typical CNF attachments to the fibers, after acetone solution.

3.3. Ni Particles Sizes and CNF Diameters

The mechanical properties of nano-composites depend not only on the mechanical properties of the constituents, but also on the size and size distribution of its nano-reinforcements [20,21]. For the diameters of CNTs/CNFs it is known that these are related to the size of the catalyst particles. The catalyst particles themselves also form a part of the composite material; in the current study the weight fraction of this phase is about 0.7 wt %. SEM and XRD analyses were employed to study the size distribution of the nanoparticles. From the SEM images local information is obtained, whereas the XRD results provide information averaged over a considerable specimen volume. Table 1 presents samples discussed in this Section as well as shows the main results.

Table 1. Samples used for size measurements (range and maximum for Ni particles size or CNF diameters).

Specimen	Solution	Ni Size Range, nm	Ni Size Max, nm	CNF Diam. Range, nm	CNF Diam. Max, nm	Test
no CNF growth	acetone	5–70	10	n/a	n/a	SEM, XRD
no CNF growth	water	5–60	20	n/a	n/a	XRD
0.7 wt % CNFs	acetone	15–115	20	—	—	SEM
5.0 wt % CNFs	acetone	—	—	5–35	10	SEM
16.0 wt % CNFs	acetone	25–115	50	15–70	30	SEM

n/a: not available; —: not tested for these values.

3.3.1. SEM Analysis

High-resolution SEM images were analyzed to estimate the Ni particle size distributions for the case of the acetone solution. First, the image was opened in a graphical editor, where the Ni particles were marked with solid ellipses or polygons, roughly outlining their contours in a separate image layer. Then, this layer was saved as a black & white image and the area of the markers were calculated in Matlab, using *bwlabel* and *regionprops* functions. Finally, diameters of equivalent circles and their distribution were determined.

Typical source images are shown in Figure 7a (Ni catalyst particles transformed from salt to metal form) and in Figure 7c (the same after growth of a small amount of CNFs barely visible in this image). The corresponding histograms showing diameters vs. their counts are shown in Figure 7b,d, respectively. For each case, 2 to 3 images were analyzed.

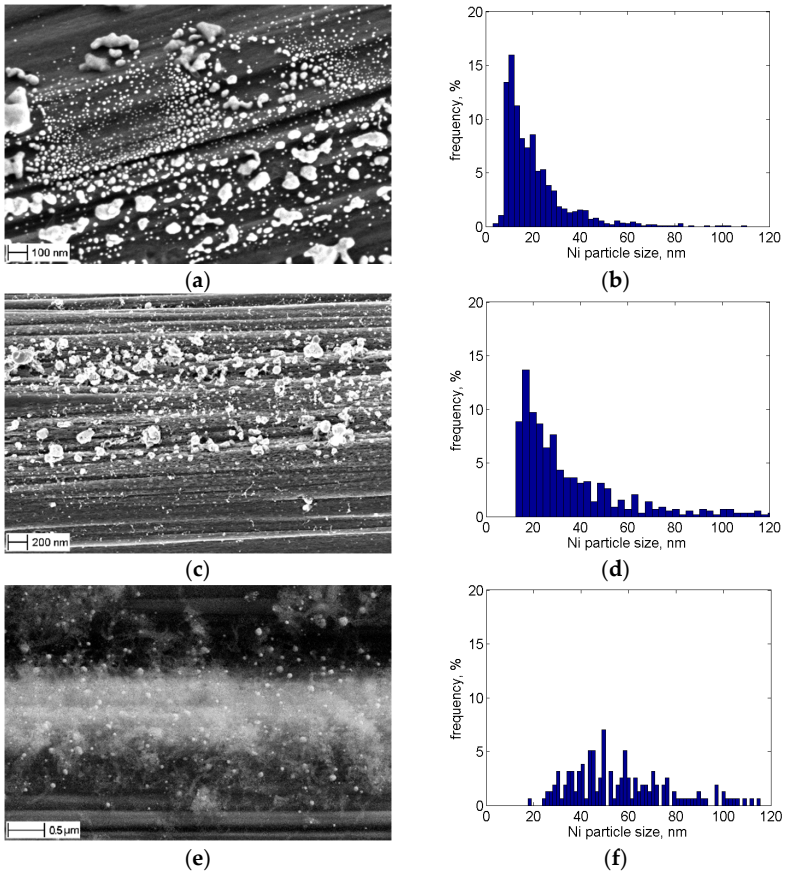

Figure 7. Ni particles in the fabric without CNF growth (**a**,**b**); or after a 0.7 wt % CNF growth (**c**,**d**); or after a 16 wt % CNF growth (**e**,**f**), acetone solution. Left—SEM images, right—calculated size distributions.

Both cases give good samples of Ni sizes and show clear peaks. In the first case the peak is situated at about 10 nm, while after CNF growth it is shifted to the right by about 10 nm. The maximal size observed (if taking the interval with, say, more than five counts) is also shifted right, by about 10–15 nm. Possible sintering occurs at elevated temperature during CNF growth leading to an increase in the size of the Ni particles and to corresponding changes in the size distributions.

Figure 7e,f shows the results of the same procedure applied for a 16 wt % CNF growth (achieved by a longer time of the growth). The high-resolution SEM picture was taken here in the "background" mode. The Ni catalyst particle sizes are within a 25–100 nm range, with the maximum at about 50 nm. Thus, comparison with Figure 7d suggests that a higher CNF growth results in a broader distribution of larger CNF diameters. Besides a possible reason mentioned above (sintering), another reason for this might be in the tip growth of CNFs mentioned earlier. Then, the larger particles have more chances to be at the top of the CNF "forest" and thus are well visible, while the smaller ones are hidden deeper.

The distributions of CNF diameters are investigated in a similar way, but the diameters are only marked with lines. Results are shown in Figure 8 and generally are similar to the Ni particles, Figure 7d,f.

However, it should be noted that the maximums of these distributions are at smaller size values than the corresponding values of the Ni catalyst particles. This might indicate for a possible "selective" growth of CNFs, when too large (and in most cases not regular-shaped as seen e.g., in Figure 7a above) Ni particles have less chances to give birth to new CNFs. Certainly fragmentation of large Ni particles also plays a role (being opposite to sintering).

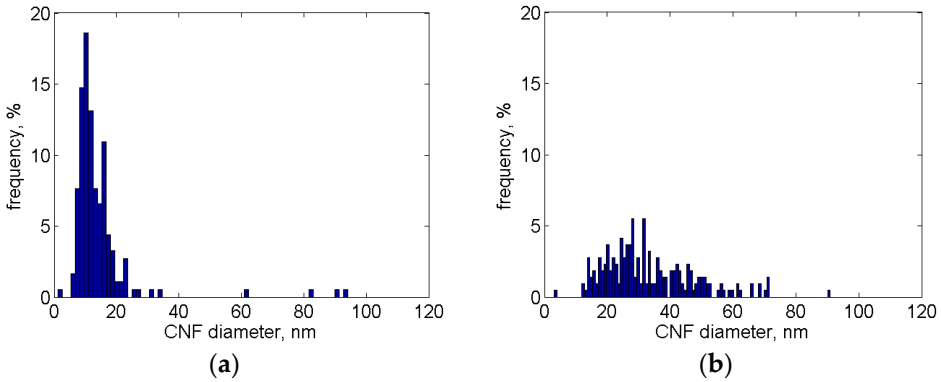

Figure 8. Distributions of CNF diameters after about 5 wt % (**a**) or 16 wt % (**b**) growth, after acetone solution.

3.3.2. XRD Analysis

In the previous section, the Ni particle size distributions were determined using the visible particles in selected regions of the samples. With X-ray Diffraction (XRD) relatively large volumes of the material can be analyzed at once. Here, the main results of such an analysis are given; detailed information will be provided in a future paper.

Typical overview diffractograms of the fabrics without and with distributed Ni particles are shown in Figure 9. Comparing the diffractograms, the reflections from the fabric and from the Ni particles can clearly be separated. Five different Ni reflections are visible, that were subsequently measured separately in more detail to allow line profile analysis.

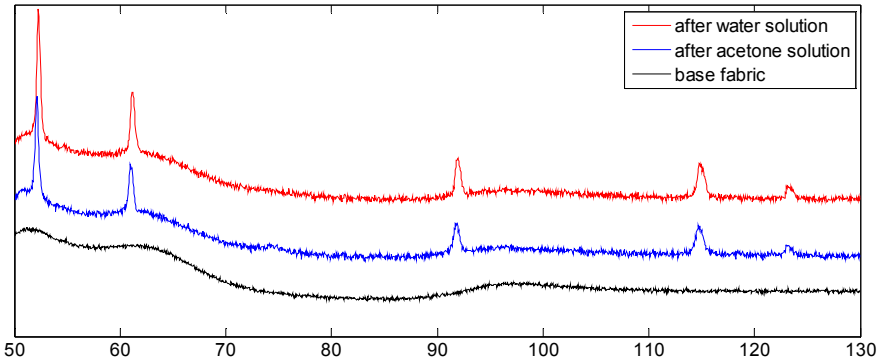

Figure 9. XRD overview scans of the base fabric before and after introduction of Ni particles on a square root intensity scale employing Co radiation. Scans are shifted vertically.

The analysis was performed by fitting of simulated line profiles to all experimental ones simultaneously assuming (i) a lognormal size distribution of spherical Ni particles distributed homogeneously through the specimens and (ii) a limited number of straight dislocations distributed over relevant Ni slip planes. The contribution from the instrument to the broadening of the reflections was determined and adequately removed from the measured Ni reflections, employing separately measured LaB_6 reflections.

Application of the profile fitting routine shows good results with only a small difference between the measured and the fitted profiles. The dislocation density is of the order of $10^{14}/m^2$. The so-obtained lognormal size distribution of spherical Ni crystallites after deposition with the acetone solution is shown in Figure 10a along with the experimentally obtained distribution from the SEM images, as described in the previous section. Both distributions are in the same range of particle dimensions, although the XRD based distribution seems to miss some of the smallest Ni particles observed with SEM. However, if one assumes that (i) the Ni crystallites have a prolate ellipsoidal shape ($r_1 = r_2 < r_3$, $r_3 = p \times r_1$) and (ii) are somewhat embedded in the carbon fiber surface with their long axis (r_3) parallel to the surface normal (see Figure 7a), fitting of the Ni reflections yields a modified lognormal Ni crystallite size distribution that complies well with the one from the SEM images (see Figure 10a). In this way, the particle dimensions determined from the visible part of the particles may differ from those determined from XRD. For the acetone-based Ni particles, it holds $p = 2.3$.

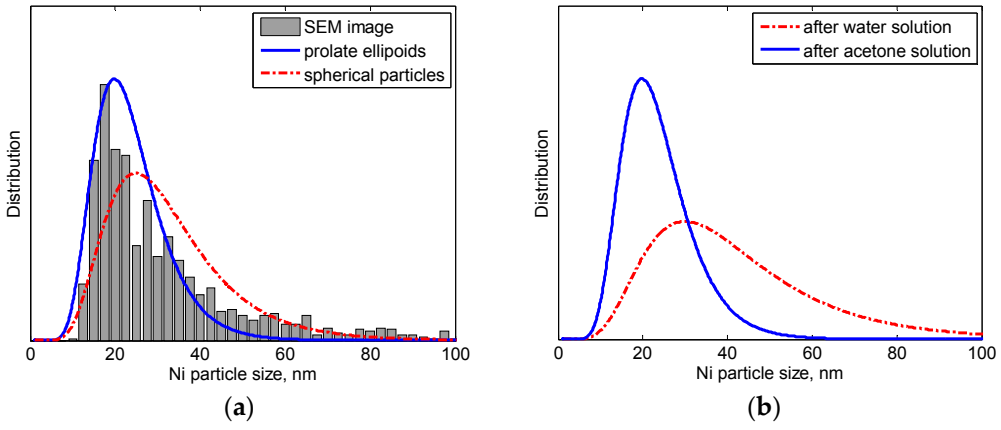

Figure 10. (**a**) Comparison of particle size distributions obtained with XRD (continuous lines) or with SEM (histogram), assuming a log normal distribution of spherical (red) or prolate ellipsoidal (blue) Ni particles. The long axis (r_3) of the prolate ellipsoids is parallel to the surface normal of the carbon fibers; (**b**) XRD particle size distributions for acetone and water-based Ni particles of prolate ellipsoidal shape.

A similar procedure was performed to determine the Ni crystallite size distribution after deposition with the water solution, with results shown in Figure 10b. The Ni reflections show less broadening, indicating a somewhat larger average crystallite size. The optimal particle shape to fit the simulated reflections is a nearly spherical shape (i.e., p = 1.15). Unfortunately, fewer Ni particles are visible in the available SEM images after the water solution, making a detailed comparison of the simulated and experimental distributions difficult.

From the SEM and XRD results, it can be concluded that the Ni crystallites have dimensions in the order of 20–50 nm. Their distributions can be described by a lognormal distribution. The XRD analysis indicates smaller dimensions for the acetone-based particles than for the water-based particles; this may possibly be attributed to lower surface tension of acetone, as well as to a different evaporation rate [2].

3.4. Erosion of Carbon Fibers

Sometimes, significant erosion is observed on the fiber surface after the reduction of Ni salt into Ni particles, Figure 11, both after the water or acetone solution. It is a known fact that Ni can catalyze erosion of a carbon substrate with reactive gasses [22]. However, this was surprising in the present study, since Ni particles were expected to lift quickly over the substrate by the growing CNFs. Maybe this separation does not occur promptly enough in the areas of agglomerates of Ni nitrate [2]. Another reason can be in a 30–45 min delay between the onset of the hydrocarbon gas mixture flow and actual growth of CNFs [2]. During this "starting up" time, Ni particles are probably still in direct contact with the fiber surface. To prove these speculations, one should vary the parameters influencing the "starting up" time and correlate it with the final structure. However, this is beyond the scope of this study.

Interestingly enough, this erosion did not occur when cold solution of urea and $Ni(NO_3)_2$ in water was used to deposit Ni onto the fabric, although the same oxidation step (drying in air) was performed as in the modified (solution heated to 90°) version of this method [2].

To check this effect in a simple way (and also to check for the amount of "burnt" sizing), several TGA (Thermogravimetric Analysis) tests were performed for the "base" fabric with or without deposited Ni nitrate, either in a reducing (N_2/H_2) or oxidizing (air) atmosphere. The heating rate was 10 °C/min in both cases.

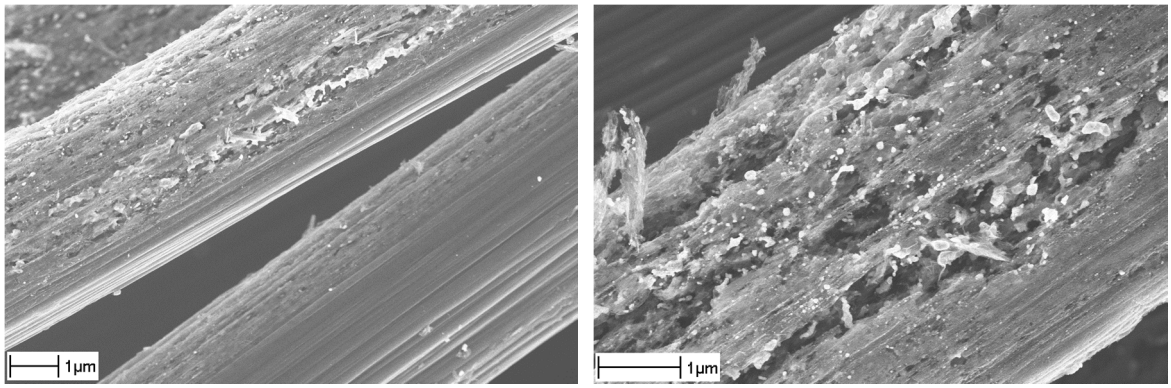

(**a**) (**b**)

Figure 11. SEM images of eroded fibers, after acetone solution: smaller (**a**) and larger (**b**) magnifications.

Results are shown in Figure 12 and indicate for a slightly larger mass loss already after 300 °C but, unexpectedly, in the fabric without Ni. A reason for this result can be in a too small specimen size (~8 mg) that could be too sensitive to the non-uniformity of sizing in the fabric meso-structure. At about 800 °C everything burns, and this total oxidation step is clearly catalyzed by Ni.

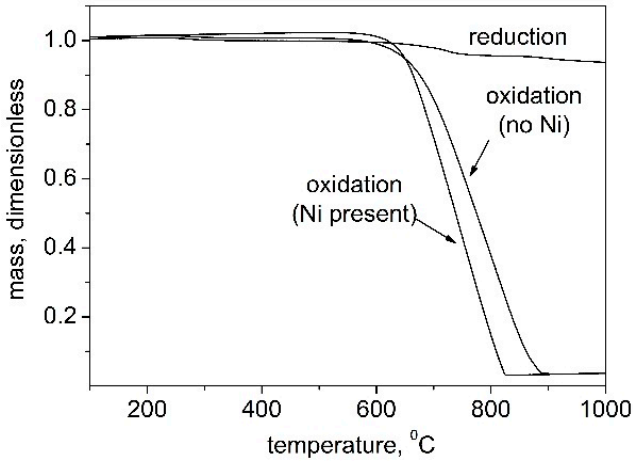

Figure 12. TGA for the "base" fabric in reducing oxidizing atmosphere.

3.5. Resulting Chemical Composition

The fiber-matrix interface plays an important role in controlling some of the mechanical properties in composites. Particularly, the strength of the interface region depends on a surface fiber treatment and resulting chemical properties of the fiber surface [23,24]. To reveal the final chemical composition of the studied material, two analysis techniques—XRF (X-ray Flourescence) and XPS (X-ray Photoelectron Spectroscopy)—were employed.

3.5.1. X-ray Flourescence Analysis

Qualitative results for the spectrum peaks are presented in Table 2. While the intensity spectrum of the base fabric is quite flat and indicates for only trace amounts of several elements, usually attributed to the specifics of the fiber production processes [25], the grafted fabrics show distinct peaks for Zn and Ni. The 7.1 wt % grafted fabric spectra indicate also for prominently increased amounts of Cr and Fe. This can be explained by migration of Zn, Cr, and Fe from the reactor walls and the gas-supplying pipes.

Table 2. Elemental components of XRF spectrum peaks (kilocounts per second), acetone solution.

	Mo	Zn	Cu	Fe	Cr	P	Ca	Sn	S	Si	Ni
base fabric	—	—	2.2	0.43	1.24	0.16	0.25	0.20	0.15	1.35	—
1.4 wt % CNFs	—	15.5	2.3	0.51	1.32	0.14	0.68	0.28	0.38	1.37	60
7.1 wt % CNFs	0.79	6.4	2.5	2.8	7.6	0.13	0.71	0.29	0.75	1.31	47

—: not detected.

It is also possible to speculate about the influence of these parasitic metals on the local erosions mentioned in the previous section, but this requires further analysis beyond the scope of this paper.

3.5.2. X-ray Photoelectron Spectroscopy Analysis

Raw data for XPS spectra are shown in Appendix, while the extracted results are presented in Table 3 and reveal that the surface chemical compositions are different before and after the heat treatments and CNF growth.

The first three elements—C, N, and O—show prominent differences in the concentrations possibly important for the composite production. For example, a significant decrease in the oxygen content (almost all surface oxygen groups are removed) can be crucial for adhesion with polymer matrices, especially with epoxies, as noticed in [25]. This decreased oxygen concentration is not surprising, because the heat treatment is performed in a nitrogen atmosphere. Thus, oxygen containing

compounds and functional groups will decompose to a higher extent when the temperature is higher (for both "desized" specimens) or the treatment time is longer (for the CNF-grafted specimen), as seen in Table 3.

Table 3. Atomic concentrations (%, mean values) of elements shown by XPS tests. Numbers in brackets indicate elements probably not present (standard deviation larger than the signal).

	C	N	O	Na	Si	Cl	Ca	Ni
sized	74.21	4.30	20.72	(0.19)	(0.07)	0.36	0.15	—
desized at 400 °C	82.76	8.38	8.31	(0.11)	(0.26)	(0.04)	(0.14)	—
desized at 600 °C	87.78	6.71	4.99	(0.12)	0.31	(0.03)	(0.05)	—
1.4 wt % CNFs, acetone solution	94.93	2.07	2.18	—	—	—	—	0.81

—: not detected.

The relatively high amount of nitrogen in the "desized" specimens can be explained as follows. It is known [26] that the sizing does not contain nitrogen and could thus "hide" it (probably originating from the carbon fiber production process) from XPS, because this technique is sensitive for a very thin surface layer only. When the "desizing" is performed, the nitrogen should therefore become more "visible". In the grafted specimen, the amount of nitrogen becomes prominently lower, probably because in this case the "desizing" is followed by the CNF-growth stage performed in a carbon-rich atmosphere (thus "hiding" the N again, as the CNFs themselves do not contain the N).

The increased amount of carbon in both "desized" specimens is believed to be due to "burning" of the sizing and its partial carbonization. In the grafted specimen, the amount of this additional carbon is then increased even more.

Absence of the metals (except for Ni) detected previously with XRF can be explained in two ways. The first reason could be that a much smaller volume of the fabric was used for XPS (about 0.2 mm^2 only), so locally smaller amounts of Zn, Cr, Cu, and Fe could be present in this volume giving signals not distinguishable from the spectrum noise. The second—probably the main—reason could be in the afore-mentioned surface character of the XPS technique (only a 5 nm surface layer is measured, vs. about a 10 μm depth in XRF), at that all the samples have been kept in ambient air before the tests and thus were covered with a thin layer of the "adventitious" carbon. In this case, all small amounts of any elements have good chances to be "hidden" under this layer, at least partially.

Beside different concentrations, the specimens show also differences in C, N, and O bondings. This is revealed by the chemical shifts in the decomposed spectra of C1s electrons. Results are presented in Table 4, for the elemental composition (%) and binding energies (eV). The first column shows the "reference" C-C*-C signal at ~284.8 eV, where "*" denotes the carbon atom in question. In the second column, a typical ~1.5 eV shift above the "reference" presumably indicates the presence of C-C*-O bonds. However, there are other possible compounds giving a similar shift, e.g., *C-C≡N. The next columns include the higher energy shifts (>2.5 eV) attributed to many more surface groups (C-C=O, O-C-O, etc.).

Generally, as follows from Table 4, while the sized fabric shows a large number of C-O bonds and a minor number of C=O bonds, other specimens show all kinds of C bonds with O or N. Similar effects have been reported in [25]. In comparison with the desizing process, the CNF growth seems to have a relatively small effect on the amount of chemical bonds.

Table 4. Carbon bond composition (%) of the fiber surfaces determined by measuring the relative areas of XPS peaks.

Functional Groups	C-C*-C	C-C*-O, etc.	N-C=O, etc.	C-C=O	O-C-O, etc.
Band Energy, eV	**ref = 284.8**	**ref + 1.5**	**ref + 3.5**	**ref + 4.5**	**ref + > 5.5**
sized	51.9	43.8	—	4.3	—
desized at 400 °C	64.9	17.6	8.0	—	9.5
desized at 600 °C	69.1	14.8	6.8	—	9.3
1.4 wt % CNFs, acetone solution	71.7	10.7	5.8	—	12.8

4. Conclusions

The main results of this study can be outlined as follows:

- CNFs can successfully be grown on a large fabric in situ with density and morphology potentially suitable for production of composites.
- Specifics of the Ni catalyst deposition process influence the uniformity of the distribution of a CNF "forest" and, to a lesser extent, its morphology; particularly, the CNF morphology depends on the catalyst loading and the solvent used for $Ni(NO_3)_2$ deposition.
- The fiber surface functional groups significantly change after the growth of CNFs.

Acknowledgments: The work was performed within the Transforce ('Transverse Reinforcement of Carbon Fiber Composites with Carbon NanoFibers') project primarily funded by STW, The Netherlands. The used fabric was kindly provided by TenCate Advanced Composites B.V.

The authors are very thankful to Mark Smithers and Laura Vargas (University of Twente) for their help with SEM, as well as to Gerard Kip (ibid) for his help with XPS tests, and to Louise Vrielink and Tom Velthuisen (ibid) for their help with XRF tests. Gert Jan Nevenzel and Ruben Lubkemann (ibid) are gratefully acknowledged for their help in specimen preparation and testing.

Author Contributions: Leon Lefferts, Remko Akkerman, Laurent Warnet, Ton Bor, Željko Kotanjac, and Vitaly Koissin conceived and designed the experiments; Vitaly Koissin and Ton Bor performed them. Vitaly Koissin and Ton Bor analyzed the data and wrote the paper.

Conflicts of Interest: The authors declare no conflict of interest. The founding sponsors had no role in the design of the study; in the collection, analyses, or interpretation of data; in the writing of the manuscript; and in the decision to publish the results.

Abbreviations

The following abbreviations are used in this manuscript:

CNFs	Carbon Nanofibers
CNTs	Carbon Nanotubes
CVD	Chemical Vapor Deposition
PPS	Polyphenylene sulfide
SEM	Scanning Electron Microscope
XRD	X-ray Diffraction
XRF	X-ray Flourescence
XPS	X-ray Photoelectron Spectroscopy

Appendix

Figures below show survey XPS spectra (Pass Energy = 224 eV, δE = 0.8 eV, 3 cycles) discussed in Section 3.5.2.

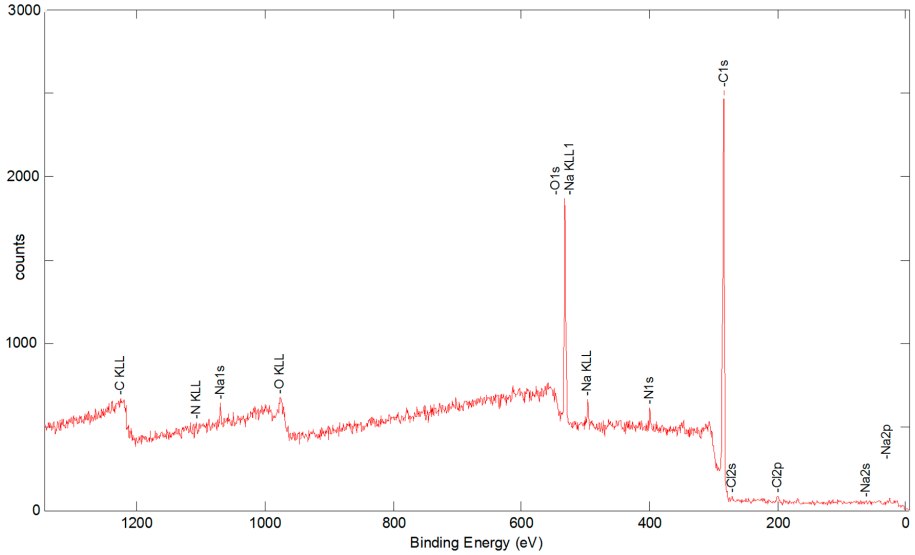

(a)

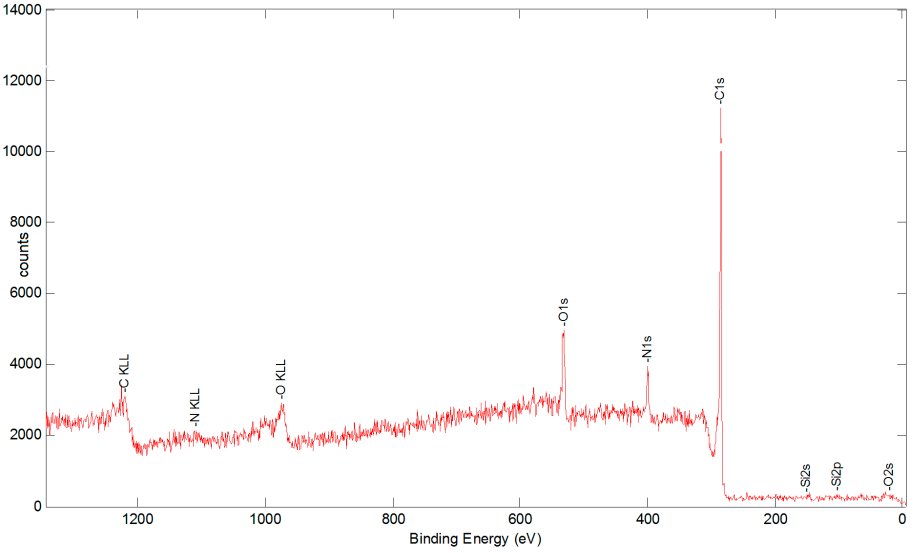

(b)

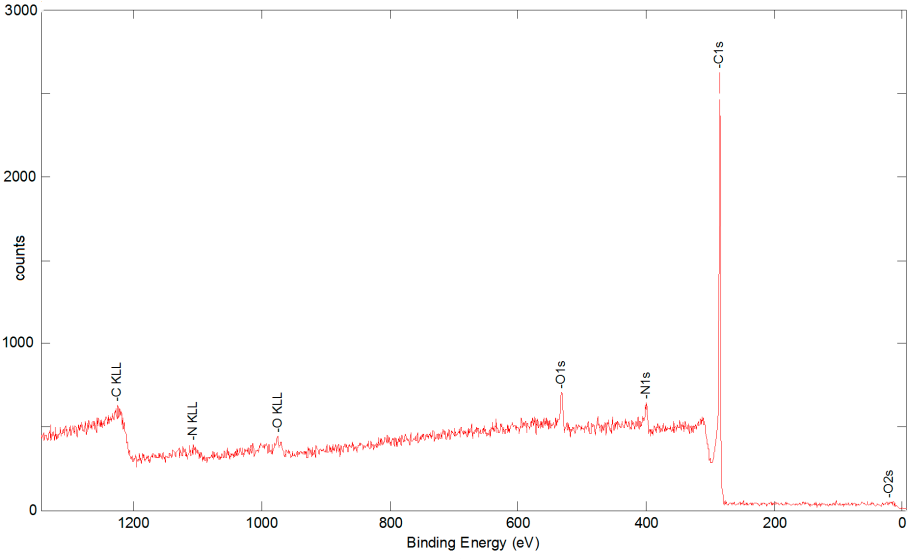

(c)

Figure A1. *Cont.*

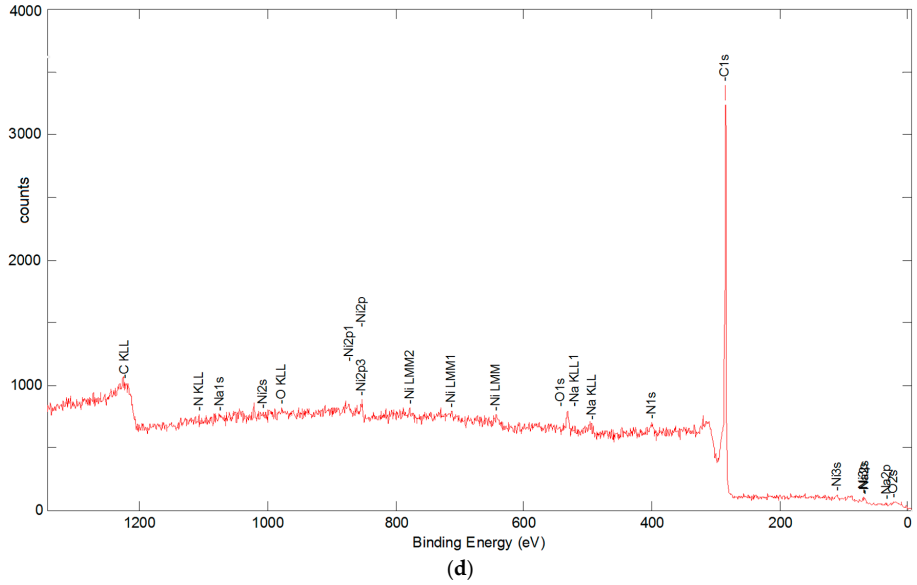

(**d**)

Figure A1. XPS spectra for sized fabric (**a**); desized at 400 °C (**b**); desized at 600 °C (**c**); or with a 1.4 wt % CNFs (**d**).

References

1. Karger-Kocsis, J.; Mahmood, H.; Pegoretti, A. Recent advances in fiber/matrix interphase engineering for polymer composites. *Prog. Mater. Sci.* **2015**, *73*, 1–43. [CrossRef]
2. Kotanjac, Ž.; Lefferts, L.; Koissin, V.; Warnet, L.; Akkerman, R. Synthesis of carbon nanofibers on large woven cloth. *C J. Carbon Res.* **2015**, *1*, 2–15. [CrossRef]
3. De Greef, N.; Magrez, A.; Couteau, E.; Locquet, J.-P.; Forró, L.; Seo, J.W. Growth of carbon nanotubes on carbon fibers without strength degradation. *Phys. Status Solidi B* **2012**, *249*, 2420–2423. [CrossRef]
4. Jia, Z. Effect of surface treatment on the structure and properties of para-aramid fibers by phosphoric acid. *Fibers Polym.* **2013**, *14*, 59–64.
5. Park, S.-J. *Carbon Fibers*; Springer: Rotterdam, The Netherlands, 2014.
6. Chen, W.; Qian, X.-M.; He, X.-Q.; Liu, Z.-Y.; Liu, J.-P. Surface modification of Kevlar by grafting carbon nanotubes. *J. Appl. Polym. Sci.* **2011**, *123*, 1983–1990. [CrossRef]
7. Lee, G.; Kim, K.J.; Yu, W.; Youk, J.H. The effect of the surface roughness of carbon fibers on CNT growth by floating-catalyst chemical vapour deposition. *Int. J. Nanotechnol.* **2013**, *10*, 800–810. [CrossRef]
8. Steiner, S.A.; Li, R.; Wardle, B.L. Circumventing the mechanochemical origins of strength loss in the synthesis of hierarchical carbon fibers. *ACS Appl. Mater. Interfaces* **2013**, *5*, 4892–4903. [CrossRef] [PubMed]
9. Zhao, Z.-G.; Ci, L.-J.; Cheng, H.-M.; Bai, J. The growth of multi-walled carbon nanotubes with different morphologies on carbon fibers. *Carbon* **2005**, *43*, 651–673. [CrossRef]
10. Tzengm, S.-S.; Hung, K.-H.; Ko, T.-H. Growth of carbon nanofibers on activated carbon fiber fabrics. *Carbon* **2006**, *44*, 859–865. [CrossRef]
11. Fan, W.; Wang, Y.; Chen, J.; Yuan, Y.; Li, A.; Wang, Q.; Wang, C. Controllable growth of uniform carbon nanotubes/carbon nanofibers on the surface of carbon fibers. *RSC Adv.* **2015**, *5*, 75735–75745. [CrossRef]
12. Ghaemi, F.; Ahmadian, A.; Yunus, R.; Ismail, F.; Rahmanian, S. Effects of thickness and amount of carbon nanofiber coated carbon fiber on improving the mechanical properties of nanocomposites. *Nanomaterials* **2016**, *6*, 1–16. [CrossRef]
13. Torayca® T300 Technical Data Sheet No. CFA-002. Avaliable online: www.toraycfa.com/pdfs/T300JDataSheet.pdf (accessed on 25 April 2016).
14. Morgan, P. *Carbon Fibers and Their Composites*; CRC Press Taylor & Francis Group: Boca Raton, FL, USA, 2005.
15. TenCate. U.S. Patent 7,252,726 B2, 7 August 2007.

16. Lomov, S.V.; Gorbatikh, L.; Kotanjac, Ž.; Koissin, V.; Houlle, M.; Rochez, O.; Karahan, M.; Mezzo, L.; Verpoest, I. Compressibility of carbon woven fabrics with carbon nanotubes/nanofibers grown on the fibers. *Compos. Sci. Technol.* **2011**, *71*, 315–325. [CrossRef]
17. Hou, Y.; Kondoh, H.; Ohta, T.; Gao, S. Size-controlled synthesis of nickel nanoparticles. *Appl. Surface Sci.* **2005**, *241*, 218–222. [CrossRef]
18. Kumar, A.; Shankar, R.; Saxena, A.; Mozumdar, S. Controlled synthesis of size-tunable nickel and nickel oxide nanoparticles using water-in-oil microemulsions. *Adv. Nat. Sci. Nanosci. Nanotechnol.* **2013**, *4*, 025009. [CrossRef]
19. De Riccardis, M.F.; Carbone, D.; Makris, T.D.; Giorgi, R.; Lisi, N.; Salernitano, E. Anchorage of carbon nanotubes grown on carbon fibers. *Carbon* **2006**, *44*, 671–674. [CrossRef]
20. Subramanian, V.; Wolf, E.E.; Kamat, P.V. Catalysis with TiO2/gold nanocomposites. Effect of metal particle size on the Fermi level equilibration. *J. Am. Chem. Soc.* **2004**, *126*, 4943–4950. [CrossRef] [PubMed]
21. Tyurin, A. Particle size tuning in silver-polyacrylonitrile nanocomposites. *eXPRESS Polym. Lett.* **2010**, *4*, 71–78. [CrossRef]
22. De Greef, N.; Zhang, L.; Magrez, A.; Forró, L.; Locquet, J.-P.; Verpoest, I.; Seo, J.W. Direct growth of carbon nanotubes on carbon fibers: Effect of the CVD parameters on the degradation of mechanical properties of carbon fibers. *Diamond Relat. Mater.* **2015**, *51*, 39–48. [CrossRef]
23. Dai, Z.; Shi, F.; Zhang, B.; Li, M.; Zhang, Z. Effect of sizing on carbon fiber surface properties and fibers/epoxy interfacial adhesion. *Appl. Surface Sci.* **2011**, *257*, 6980–6985. [CrossRef]
24. Luo, U.; Zhao, Y.; Duan, Y.; Du, S. Surface and wettability property analysis of CCF300 carbon fibers with different sizing or without sizing. *Mater. Des.* **2011**, *32*, 941–946. [CrossRef]
25. Hammer, G.E.; Drzal, L.T. Graphite fiber surface analysis by X-ray Photoelectron Spectroscopy and Polar/dispersive Free Energy Analysis. *Appl. Surface Sci.* **1980**, *4*, 340–355. [CrossRef]
26. Reis, M.J.; Botelho Do Rego, A.M.; Lopes Da Silva, J.D.; Soares, M.N. An XPS study of the fiber-matrix interface using sized carbon fibers as a model. *J. Mater. Sci.* **1995**, *30*, 118–126. [CrossRef]

© 2016 by the authors; licensee MDPI, Basel, Switzerland. This article is an open access article distributed under the terms and conditions of the Creative Commons Attribution (CC-BY) license (http://creativecommons.org/licenses/by/4.0/).